applied sciences

MDPI

Article

Hydrogen Intramolecular Stretch Redshift in the Electrostatic Environment of Type II Clathrate Hydrates from Schrödinger Equation Treatment

Christian J. Burnham [1,*], Zdenek Futera [2], Zlatko Bačić [3,4] and Niall J. English [1,*]

1 School of Chemical and Bioprocess Engineering, University College Dublin, Belfield, 4 Dublin, Ireland
2 Faculty of Science, University of South Bohemia, Branisovska 1760, 370 05 Ceske Budejovice, Czech Republic; futera.zd@gmail.com
3 Department of Chemistry, New York University, New York, NY 10003, USA; zlatko.bacic@nyu.edu
4 NYU-ECNU Center for Computational Chemistry at NYU Shanghai, 3663 Zhongshan Road North, Shanghai 200062, China
* Correspondence: christianjburnham@gmail.com (C.J.B.); niall.english@ucd.ie (N.J.E.)

Received: 30 October 2020; Accepted: 24 November 2020; Published: 28 November 2020

Abstract: The one-dimensional Schrödinger equation, applied to the H_2 intramolecular stretch coordinate in singly to quadruply occupied large cages in extended Type II (sII) hydrogen clathrate hydrate, was solved numerically herein via potential-energy scans from classical molecular dynamics (MD), employing bespoke force-matched H_2–water potential. For both occupation cases, the resultant H–H stretch spectra were redshifted by ~350 cm^{-1} vis-à-vis their classically sampled counterparts, yielding semi-quantitative agreement with experimental Raman spectra. In addition, ab initio MD was carried out systematically for different cage occupations in the extended sII hydrate to assess the effect of differing intra-cage intrinsic electric field milieux on H–H stretch frequencies; we suggest that spatial heterogeneity of the electrostatic environment is responsible for some degree of peak splitting.

Keywords: hydrogen; clathrate hydrate; cages; confinement; nuclear quantum effects; redshift; Schrödinger; electric field

1. Introduction

A clathrate hydrate is a crystalline inclusion compound with a structure consisting of "big" and "small" cavities formed from polyhedra. A host lattice is composed of water molecules which are hydrogen bonded, joining the cavities by connections to each cage's vertex [1]. The cavities can, and do, entrap guest atoms and molecules. Type II (also termed "sII") hydrates comprise a series of big cavities of type $5^{12}6^4$ (featuring 12 faces formed by pentagons, and 6 by hexagons) and small-cavity 5^{12} dodecahedra, each featuring 12 water pentamers. In the case of hydrogen hydrates, cavities may hold differing numbers of H_2 molecules [1]. Although on short timescales H_2 guests appear to be trapped permanently in particular cages, it is possible for them to hop between cavities on longer timescales, such that they diffuse throughout the lattice [2–12]. H_2 hydrates are of much practical interest as they display many interesting properties as an attractive material for the storage of hydrogen [13–21]. At 0.2 GPa, it was determined by Mao et al. that mixtures of hydrogen and water form crystals as sII clathrates with a hydrogen accommodation level of 5.3 wt.% at 0.3 GPa and −23 °C—not far at all from the ambition of 5.5 wt.% expressed by the United States Department of Energy [21].

In any event, the intra-cage environment of hydrates constitutes an intriguing playground for dissecting the vagaries of caged H_2 behavior, especially spectroscopic and dynamical, which can be strongly quantal in nature, arising from nuclear quantum effects (NQEs) from various possible

backgrounds. For instance, the center of mass (c.m.) of the guest molecule(s) is quantized in its translational degrees of freedom (DOFs) as a result of being trapped at the nanoscale in hydrate cavities, whether large or small (i.e., the "particle-in-a-box" phenomenon). The rotational DOFs of the hydrogen molecule(s) are quantized as well: these are connected with the potential of the cavities which serve to confine the quantized translational DOFs. This gives rise to sparsity in energy levels in translation–rotation (TR) due to the low mass of H_2, its substantial rotational constant, and the hydrate cages' small size. On the theoretical side, TR eigenstates depict notable properties for a single hydrogen molecule in the ground vibrational state in the cages of sII clathrate hydrate (treated as rigid), and this has been characterized by Bačić and co-workers via quantum five-dimensional computations in the bound state [22–25], alongside calculation to a rigorous standard of the associated inelastic neutron-scattering spectra [26–31]. For a small-cage-confined H_2 molecule, the sII hydrate theoretical results' key aspects are in quantitative agreement with the inelastic neutron scattering (INS) [32] and rotational Raman spectra [33,34] of these systems.

For up to four vibrational-ground-state hydrogen molecules in the $5^{12}6^4$ cages, their quantum TR dynamics have been probed at T = 0 K via diffusion Monte Carlo [35] and path integral molecular dynamics approaches [2–4,36] over a range of temperatures, alongside computations employing full coupling and resolution of eigenstates for two [37,38] and four caged H_2 molecules [39].

Another spectroscopic manifestation of hydrogen molecule entrapment in clathrate cages is the frequency shift of their H–H stretch vibration vis-à-vis the in vacuo result. This is obvious from Raman-mode analysis for mixed sII tetrahydrofuran/H_2 clathrate, in which the $5^{12}6^4$ cavities are occupied fully by THF whilst single H_2 occupancy of 5^{12} cages is obtained, and also for the case of "pure" sII clathrates, wherein H_2 molecules are the sole guests [34,40]. These entrapped molecules' H–H stretch modes are always reduced in frequency compared with their in vacuo counterparts, i.e., redshifted vis-à-vis gas-phase results. The most prominent such shift, −34 cm^{-1}, was witnessed in the sII THF/H_2 clathrate's Raman modes, arising clearly for the singly occupied 5^{12} cavity [34,40]. An identical redshift was prominent in the case of pure sII H_2 clathrates, rendering it unambiguous that this arises due to H_2's presence in the 5^{12} cavities.

Pure H_2 hydrate spectra depicted mode shifting by −26, −18, and −11 cm^{-1} [34,40], denoting contributions from $5^{12}6^4$ cavities with H_2 occupations between two and four. Highly controlled, accurate, and sophisticated experiments, entailing several heating and quenching cycles with careful measurements of H_2 amounts released in each, resulted ultimately in the attribution of these respective redshifts to double, triple, and quadruple $5^{12}6^4$ cage occupations [40]. The H–H stretch shift can be rationalized as an effective coupling between two types of interactions [40]. Of these, one, i.e., the attractive interaction between H_2 and the cavity, softens the H–H stretch potential and reduces its value vis-à-vis the result in vacuo. With increasing $5^{12}6^4$ cavity occupation, there is, naturally, closer H_2–H_2 packing, and these essentially repulsive H_2–H_2 interactions result in a rising H–H stretch mode and a decline in the extent of redshift. The vibrational H–H mode is redshifted even for the quadruple occupation case in the $5^{12}6^4$ cavity, indicating that the predominantly attractive guest–host interactions dominate over repulsive H_2–H_2 ones.

Accurate calculation of the intramolecular vibrational frequencies of the H_2 molecule(s) inside the hydrate cages has proven to be a most challenging problem. In the last decade or so, various methodologies entailing a range of approximations have been adopted to tackle this challenging conundrum. In one approach [41,42], the cage-entrapped hydrogen molecules were treated as frozen in the minimal-energy geometry corresponding to the minimum energy of the system and at 0 K. Consequently, nuclear quantal effects were neglected—indeed, most pointedly in the case of "smearing out" the guests' large-amplitude vibrations. Moreover, given that only isolated cavities were modelled, the surrounding condensed-matter milieu's influence was not taken into account. To tackle this omission of the background lattice, a judicious mixture of both classical and path integral molecular dynamics (MD and PIMD) simulations employing Density-Functional Theory (DFT) at hybrid-functional level (B3LYP) and second-order Moller-Plesset perturbation (MP2) prescriptions was used [43]. The H–H

stretch modes found under 1D conditions for the H_2 coordinates sampled from many MD simulation snapshots encapsulated a wide spread of frequencies extending to the free molecule at 4155 cm^{-1}. Indeed, the distributions' peaks were reasonably consistent with experimental values after a scaling factor was employed in the simulations [43]. Drawing from experiments in [44], classically propagated MD calculations employing DFT were carried out for a full sII clathrate unit cell, and the H–H stretch spectra were computed via Fourier transformation of the H–H bond length autocorrelation [45]. A shortcoming of this approach is the classical treatment of the underlying dynamics, leading to an overestimation of the H–H stretch modes by ~250 cm^{-1} vis-à-vis Raman measurements at 260 K.

Various flavors of PIMD, e.g., centroid and ring-polymer approaches, are of use in modelling the dynamical vibrational properties of fluids and materials, capturing, in some cases, semi-quantitative agreement with experimental results [46–48]. Strictly, however, the use of these methods is less appropriate for estimating time-dependent properties and correlation functions, as argued with acuity by Hele et al. in the formulation of Matsubara dynamics [49] and its formal relationship with forms of PIMD [50]; Matsubara dynamics may, in time, be shown to offer one pathway towards more rigorous and pragmatic approximations for quantal dynamics [50].

In principle, the most appropriate and rigorous quantal treatment of the H–H intramolecular stretch vibrational dynamics involves high-dimensional quantum calculations, with full coupling, of the vibration–rotation–translation (VRT) eigenstates of one or more H_2 molecules confined inside a clathrate hydrate cage. Such calculations face two serious obstacles. One is tackling the high dimensionality of the quantum bound state that requires a solution even when a clathrate hydrate is treated as rigid; it is $6n$, with n as the number of H_2 molecules in the hydrate cage. A second obstacle hinges on the belief, widely held until recently, that molecular systems featuring both high-frequency intramolecular vibrational mode(s) and low-frequency intermolecular ones would present a hugely difficult and computationally prohibitive task; this centers on H_2 in hydrate cavities and hydrogen-bonded/van der Waals (vdW) complexes, with rigorous computation of fundamental (and overtone) excitation(s) of their intramolecular vibrational mode(s). The principal source of this challenge was thought to be the large number of highly excited intermolecular vibrational eigenstates in the manifold of intramolecular ground states located below the energy of the intramolecular vibrational excitation(s), together with assumptions that convergence is required to afford their accurate calculation.

However, recently [51] it was shown, contrary to this expectation, that accurate calculation of the small-cage-bound H–H stretch fundamental in sII hydrate at ~4100 cm^{-1} needs only a modest number of converged TR states in the v = 0 manifold up to no more than 400–450 cm^{-1} above the ground state, and certainly none within several thousand wave-numbers of the intramolecular fundamental. This unexpected conclusion was rationalized by very weak coupling of excited intermolecular v = 0 TR states in the locale of the H_2 stretch fundamental, despite their large number. Therefore, excluding these in calculations affects the accuracy of calculating intramolecular vibrational excitation in a negligible manner. Naturally, this resulted in a substantial drop in the basis size needed and converted a computationally Herculean project into a readily tractable undertaking [51]. For the biggest (rigid) clathrate domain modelled, featuring 76 water molecules (i.e., constituting the first three hydration shells around H_2), the mode change of −43 cm^{-1} for H_2 is just 14% away from the experimental value at 20 K.

The above insight is at the heart of the rigorous and efficient methodology allowing full-dimensional quantum computations, with full coupling, of the intra- and intermolecular rovibrational states of dimers of molecules featuring weak intermolecular bonding [52]. This methodology was utilized to calculate the H–H stretch fundamentals of $(p\text{-}H_2)_2$ inside the 51264 cavity [53]. The 8D quantum methodology is predicated on rotationless (j = 0) hydrogen moieties and a frozen host lattice, but coupled fully in every other sense. The largest hydrate domain considered had 98 H_2O molecules, all those featuring O atoms within 9 Å of the center of the cage. In this case, both H–H stretch fundamental modes were observed to be site-split by ~0.5 cm^{-1} and shifted by approximately 24 cm^{-1}, i.e., in good accord with the experimental result of 26 cm^{-1}.

In both calculations [51,53], the Potential-Energy Surface (PES) employed was pairwise additive, using the ab initio hydrogen–water pairwise potential for flexible hydrogen and rigid water, and for $(H_2)_2$, the 6D H_2–H_2 PES.

While great strides have been made recently in the rigorous high-dimensional quantum bound-state treatment of H-H intramolecular stretching excitations [51,53], serious limitations remain. The results obtained are for T = 0 K. The hydrate domains included in the calculations are treated as rigid, precluding any coupling between the hydrate phonons and the H-H intramolecular stretch, and its temperature dependence. Only one cage, small or large, is occupied by the H_2 molecule(s), while all other cages in the considered domain are left empty. Consequently, the effects of interactions between the H_2 molecules in neighboring cages cannot be explored (although they are expected to be very small).

In the present study, bearing in mind these limitations, as well as the limitations of other, less rigorous approaches outlined above, we are motivated to rigorously solve the one-dimensional Schrödinger equation in the singly occupied large-cage case, as well as, to a good level of approximation, for the doubly to quadruply occupied cases. To do so, we employ the extended sII solid as well as using a state-of-the-art potential model parameterized directly from force-matching ab initio, electronic-structure-based MD propagated classically with high-quality DFT [4]. This model has been shown to be accurate, and it allows for a more rigorous treatment of nuclear quantum effects. We are also curious as to the potential relationship, if any, between intrinsic electric fields present in hydrates [54,55]—which will inevitably display some form of spatial heterogeneity within cavities—and H–H stretch frequencies per se; non-uniformities in electrostatic intra-cage milieux may possibly influence intramolecular vibrational properties.

2. Methodology

Born–Oppenheimer (BO)-MD simulations were performed under periodic boundary conditions (PBC) using a vdW-DF dispersion functional based on generalized gradient approximation (GGA) employing Dion-Rydberg-Schröder-Langreth-Lundqvist (DRSLL) non-local correlation correction [56,57]. This functional was recently shown to perform exceptionally well for liquid water [58–63] and has also yielded realistic results for the H_2-hopping free-energy barrier in H_2 hydrates [3] and Raman vibrational properties vis-à-vis experimental results [45]. The simulations were performed with a time step of 0.2 fs in a canonical (NVT) ensemble. The system temperature was imposed at 258 K using a Nosé-Hoover thermostat [64,65] with fictitious mass 120 Ry.fs^2. The charge density, described in the DZP basis set, converged to an accuracy of 10^{-4} a.u at each MD step. The calculations were performed using the electronic structure software package SIESTA [66]. The ab-initio (AI)-MD trajectories were run for 5 ps at 258 K on a single unit cell in the NVT ensemble for large cage occupation numbers of $n = 1, \ldots, 4$ and single occupation of small cages for each and every cage. In addition, the case of an almost-empty lattice with a solitary H_2 molecule in just one large cage was also simulated at 258 K, with the lattice both entirely free and held rigid, so as to determine if H–H peak-splitting occurs for just a single H_2 molecule (eliminating H_2–H_2 interactions in multiply occupied cages, and even those weaker ones from neighboring cages) and the role, if any, that a mobile, vibrating lattice may have on this. Each structure was first run in the NPT ensemble at 258 K and 2 kbar beforehand to equilibrate to experimentally relevant conditions [35], producing equilibrium cell lengths of 16.5–16.6 Å. In the present study, all calculations, including those with empirical models (vide infra), were performed with a 16.6 Å cell length, consistent with DFT results.

We wish to solve Schrödinger's equation for the one-dimensional H–H stretch coordinate

$$\hat{H}\left|\psi_{\backslash}\right\rangle = \epsilon_{\backslash}\left|\psi_{\backslash}\right\rangle \tag{1}$$

where $\hat{H}$ is the Hamiltonian. Suppose we have a reference Hamiltonian, $\hat{H}^0$, satisfying

$$H^0\left|\chi_{\rangle}\right\rangle = \zeta_{\rangle}\left|\chi_{\rangle}\right\rangle \tag{2}$$

where χ_i terms have analytical solutions. Ideally, the reference Hamiltonian is chosen to be not too dissimilar from the original Hamiltonian $\hat{H}$. We can use the states of the reference Hamiltonian as an orthonormal basis in which to expand

$$\sum_j \langle \chi_\rangle | \hat{H} | \chi_j \rangle \langle \chi_\rangle | \psi_\backslash \rangle = \epsilon_\backslash \langle \chi_\rangle | \psi_\backslash \rangle \tag{3}$$

Indeed, defining

$$H_{i,j} = \left\langle \chi_\rangle \middle| \hat{H} \middle| \chi_j \right\rangle \text{ and } a_{n,i} = \left\langle \chi_\backslash \middle| \psi_\backslash \right\rangle$$

we have

$$\sum_j H_{i,j} a_{n,j} = \epsilon_\backslash a_{n,j} \tag{4}$$

Here, the eigenvalues are the energy levels; the eigenvectors can be used to reconstruct the eigenfunctions associated with each energy level. In practice, the $H_{i,j}$ matrix elements are calculated up to a reasonable maximum value of *i*,*j*, which can then be diagonalized to obtain the eigenvectors and eigenvalues.

For H–H stretch modes, a natural basis choice is provided by the eigenfunctions of the quantum harmonic oscillator, which, in the χ representation, are given by

$$\chi_n(\Delta x) = \frac{1}{2^n n!}\left(\frac{\alpha}{\pi}\right)^{\frac{1}{4}} \exp\left(-\frac{\alpha \Delta x^2}{2}\right) H_n\left(\sqrt{\alpha}\Delta x\right). \tag{5}$$

For n = 0, 1, 2, … with associated eigenvalues $\chi_n = (n + 1/2)h\omega_0$, where Δx is the displacement from the minimum ($\Delta x = x - x_0$) and $\alpha = h\omega_0/m*$, where m* is the reduced mass and ω_0 is the harmonic oscillator frequency, chosen at the outset to be close to the curvature of the potential minimum. $H_n(y)$ terms are Hermite polynomials, given by $H_0(y) = 1$ and $H_1(y) = 2y$, with higher polynomials given by recursion:

$$H_{n+1}(y) = 2yH_n(y) - 2nH_{n-1}(y). \tag{6}$$

The $H_{i,j}$ matrix elements are the sum of kinetic and potential parts:

$$H_{i,j} = KE_{i,j} + V_{i,j} \text{ where } KE_{i,j} = \left\langle \chi_\rangle \middle| \hat{KE} \middle| \chi_j \right\rangle \tag{7}$$

which have analytical solutions

$$KE_{i,j} = \frac{h\omega_0}{4}\left[\delta_{i,j}(2i+1) - \delta_{i,j-2}\sqrt{j(j-1)} - \delta_{i-2,j}\sqrt{i(i-1)}\right], \tag{8}$$

and the matrix elements of the potential are

$$V_{i,j} = \left\langle \chi_\rangle \middle| \hat{V} \middle| \chi_j \right\rangle = \int_{-\infty}^{\infty} V(x)\chi_\rangle(x)\chi_j dx \tag{9}$$

which are determined numerically.

To generate representative configurations, we ran standard classical MD at 100 K under the NVT ensemble for a unit cell, as described above for BOMD, in the case of single to quadruple occupation of the large cages (single for the small ones) using the force-matched potential of ref. [4] with the Ewald approach for long-range electrostatics [67]. From successive regular snapshots, for all H_2 molecules, we scanned over their bond distances r to generate potential curves $V(r_m)$, where V is the total potential energy of the simulation cell (under PBC, with Ewald) and r_m is the mth H_2 molecule's bond distance. The centre of mass (COM) of each H_2 molecule was kept fixed, and its bond vector was kept parallel to its initial direction (i.e., its direction in the snapshot); all other atomic coordinates remained

fixed. The spectral frequency of the oscillator was calculated from the 0->1 transition $\omega = (\epsilon_1 - \epsilon_0)/h$, with the total spectrum averaged over all oscillators (i.e., all H_2 molecules) and snapshots.

For comparison, classically sampled H–H spectra were calculated from a power spectrum of H–H bond distances from classical MD with the force-matched potential of ref. [4]. The classical power spectrum was Fourier transformed as

$$g(\omega) = \sum_m \left| \mathcal{F}\left\{ \dot{r}_m(t) \right\} \right|^2 \tag{10}$$

where $\dot{r}_m(t)$ is the H–H distance time derivative. This formulation was also applied to BO-MD, given that these dynamics are, by definition, propagated classically.

3. Results and Discussion

Figure 1 depicts the Schrödinger and classical MD sampled H–H spectra for the four large-cage occupations. A systematic redshift of ~350 cm^{-1} is clearly evident for the quantum case vis-à-vis its classical counterpart for all occupations, regardless of cage occupation or type (cf. Figure 2). This puts the Schrödinger-solved H–H stretch results in slightly superior agreement with Raman-measured data at 260 K of ~4050–4150 cm^{-1} [34,45,50], although these quantal results systematically underpredict H–H stretch modes, whilst classical MD overpredicts. This "reversed error sign" situation is not altogether ideal if one seeks true quantitative accuracy, but several mitigating factors must be borne in mind in this respect. Although ref. 4 presents a relatively accurate pairwise potential model, it is, of course, imperfect and cannot capture all of the subtleties of H_2–H_2 and H_2–water interactions. Although care has been taken to define the H–H stretch coordinate, there may be some residual background translational and rotational H_2 motion; for the case of quadruple occupation, with the H_2 molecules more localized spatially—essentially "hemmed in" to their tetrahedral configuration [2,3,35,36]—this point is less of a difficultly. Naturally, depending on occupation, one to four independent one-dimensional Schrödinger equations are solved per large cavity, and it is assumed that each H–H vibration is independent of others. This assumption may be somewhat questionable and serves to further explain the lack of full quantitative agreement with experimental results [34,40,45]. Of course, the distribution of experimental cage occupations is not well characterized or known [34,40,45], which hampers further attempts for quantitative comparison between measured Raman spectra and H–H vibrational spectra; in the present work, and the DFT-based work of ref. [45], there were found to be distinct and distinguishable differences between large-cage frequency modes and occupations (as will be discussed below). Interestingly, there was no evidence of peak "bifurcation" or splitting in each cage type, except for the case of quadruple occupation in the large cage for classical MD, which was suppressed in the Schrödinger case. Of course, to study mode-splitting effects with greater rigor, state-of-the art DRSLL is very helpful, albeit that PIMD or a Schrödinger equation approach therewith would be very computationally demanding (as discussed further below).

Figure 3 shows BO-MD-sampled H–H spectra for large-cage occupancies of 1–4, with single small-cavity occupation; here, the dynamics are propagated classically. The total spectrum is shown, in addition to individual large- and small-cage spectral decompositions. For all occupations, as with the empirical model results of Figures 1 and 2, the low-frequency part of the vibrational band originates from H_2 entrapped in small cages, whilst the large-cage hydrogen molecules contribute to the higher-frequency peaks. This clearly demonstrates the important effect of the molecular environment in influencing the spectral pattern. As discussed in ref. 45, the ratio of the peak areas corresponds to number of the H_2 molecules located in the large/small cages. Study of the broad panoply of individual-molecule spectra is revealing (cf. the lower insets for each occupation case in Figure 3). For some H_2 molecules, single-occupation spectra in the large cages (top left) show some evidence of peak splitting, as do those in small cavities for all large-cage occupancies (with single occupation therein irrespective of large-cage occupancy). However, it must be noted that no such fundamental H-H stretch

splitting was observed in quantum 6D calculations of H_2 in both small and large cages [51]; we remark on possible reasons for potentially spurious peak splitting below. Returning to the present work, even for the total, aggregate spectra (top panels in Figure 3), there is a broader distribution and heterogeneity in peaks vis-à-vis the empirical model case (cf. Figure 1). In the case of multiple large-cavity occupancy, there is less evidence of peak-splitting in individual molecules, particularly at higher occupations (cf. blue curves in Figure 3 in comparison to the single-occupancy case on the top left). This suggests an environmental effect of spatial heterogeneity within the cavities in determining, or at least influencing, the H–H vibrational frequency properties. With increasing large-cage occupation, the greater spatial localization of H_2 molecules into a quasi-tetrahedral arrangement [2,3,35,36] leads to less ability to move freely within the cavity, sampling it in a reasonably uniform way; this implies that the local electrostatic environment, possessing its own largely lattice-determined (and slightly temporally fluctuating) intrinsic electric field [54,55] at each molecule's proximal location, may determine underlying H–H stretch modes. Certainly, the broad spread of individual-molecule peaks (blue curves in the lower insets of Figure 3) points to the heterogeneity of intrinsic electric field distributions [54,55].

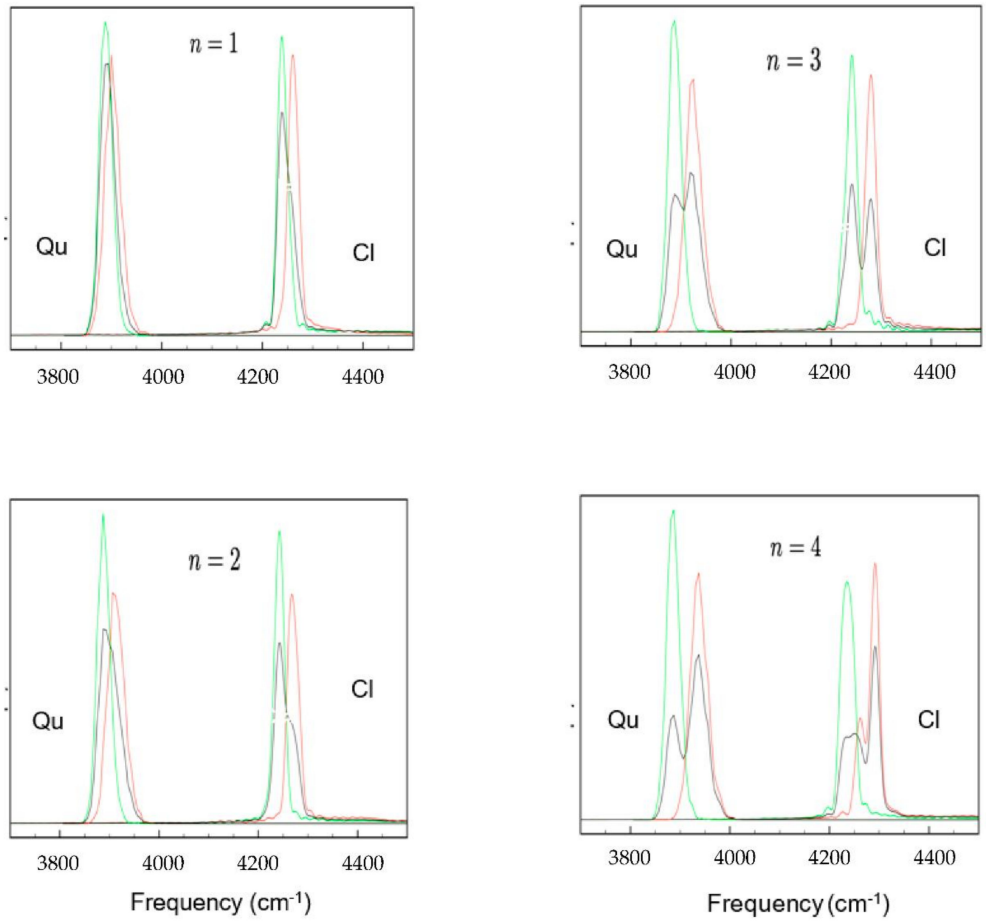

Figure 1. Schrödinger H–H spectra for large-cage occupations of $n = 1, \ldots, 4$ at 100 K, with classical molecular dynamics (MD) results. Black lines represent total spectra over all H_2 molecules, red lines represent spectra of large-cage H_2, green lines represent spectra of small-cage H_2. "Qu" refers to quantum, while "Cl" denotes classical.

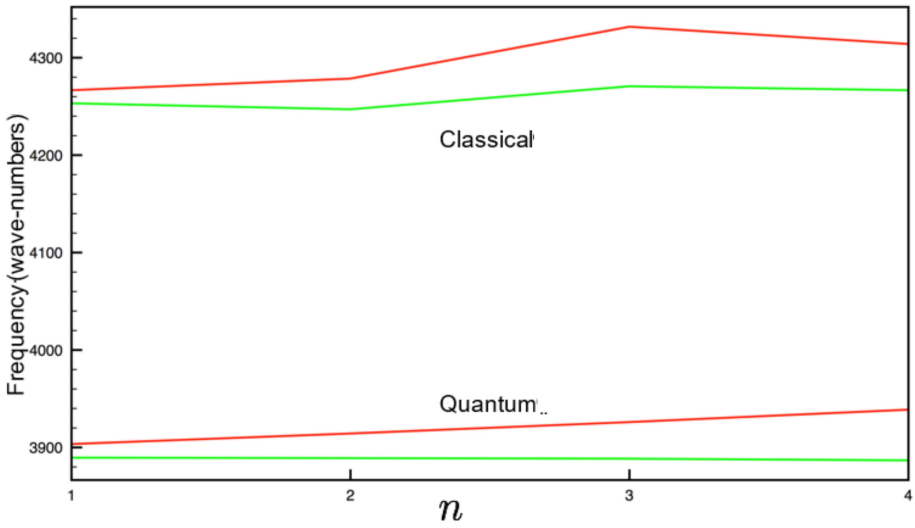

Figure 2. Average frequency positions for classical and Schrödinger large-cage (red) and small-cage (green) spectra.

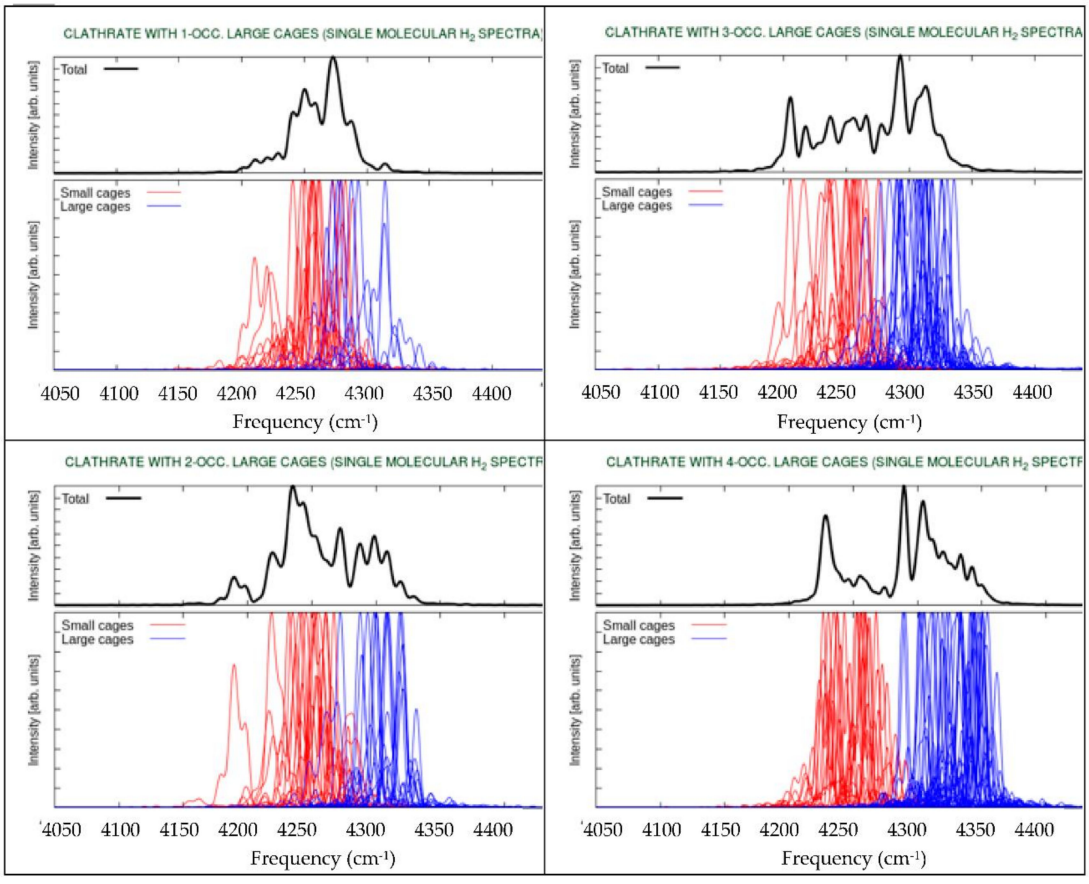

Figure 3. BO-MD-sampled H–H spectra for large-cage occupancies of 1–4, with single small-cavity occupation. Below the total spectrum is shown the large/small individual-cage spectral decomposition.

However interesting—and even appealing—this hypothesis may be of local electrostatic conditions and the electric field environment in influencing H–H stretch frequencies, it is still somewhat tentative. For instance, we have not yet been able to remove H_2–H_2 interactions, even in neighboring cages in single-occupancy cases; naturally, this may well be important for multiply occupied large cages

in determining environmental effects (albeit more in terms of structural localization, rather than electrostatic effects). With this in mind, and recalling the pivotal role of the lattice in determining local electric field intensities, we present in Figure 4 the H–H spectra for a solitary H_2 molecule in a large cage, with the rest of the unit cell cages empty, for both the mobile (normally vibrating) lattice and its fixed counterpart. It is readily evident that mode-splitting does indeed occur, to some extent, as the H_2 molecule samples space in the large cage essentially uniformly [2,3,35,36]. The ~4325 cm^{-1} peak dominates at the cage centre, but the ~4280–4310 cm^{-1} peaks are suggestive of the lesser amounts of time spent in the other "rim" of the centre, closer to the cage faces, with its more confined environment. However, we remark that in the 8D quantum calculations of ref. 53, there was no splitting of the H-H stretch fundamental observed for a single H_2 molecule in the large cage, and we discuss further potential shortcomings of splitting observations below. In any event, these observations of Figure 4 are more akin to the to-lower-frequency redshift witnessed in moving to a single H_2 molecule in a small cavity, i.e., to ~4250 cm^{-1}, featuring more intimate contact with the surrounding water molecules and cavity faces, and the enhanced intrinsic electric field intensity in this small cage borne of these stronger interactions with the lattice. Lattice rigidity, which is, of course, simply a "proof-of-concept" device here (not purported to represent rigorous physical reality), shows a dramatic direction reversal of the more minor, bifurcated peak—a blueshift to ~4430–4350 cm^{-1}, without any real movement of the main vibrational peak. The lack of principal peak shift reflects the fact that the H_2 molecule spends most of its time in the large cage's center for the single-occupation case [2,3,35], which is hardly impacted in its local electrostatic environment by lattice rigidity; conversely, the secondary peak blueshift serves as confirmation that these peaks arise from intimate water–H_2 interactions characteristic of the outer rim of H_2 localization likelihood, closer to the cage faces [2,3,35]. As argued in refs. [54,55], electric field intensity is related directly to the magnitude of Coulombic forces, which are, of course, more substantial for closer cage face/H_2 interactions.

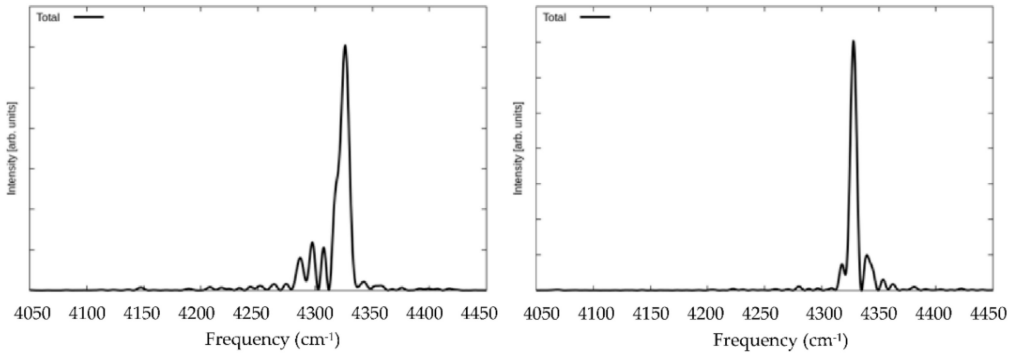

Figure 4. BO-MD-sampled H–H spectra for a solitary H_2 molecule in a large cage, with the rest of the unit cell cages empty. (**a**) Mobile lattice; (**b**) fixed lattice.

We note that this hypothesis of an increasing level of vibrational frequency redshift with increasing effective local, intrinsic electric field intensity within cage environments, particularly in small cages and near cavity faces, borne of more intimate, larger-force H_2–water interactions, is entirely consistent with the decline in MD-based DRSLL H–H stretch frequency from 4382 cm^{-1} in the gas phase [45] (with essentially negligible field) to 4270–4330 cm^{-1} (large cage) and 4250–4260 cm^{-1} (small cavity), with local fields of ~2 V/Å [54,55]. Aside from the matter of de facto electric fields (the sum of intrinsic and externally applied ones) specifically affecting H_2 stretch dynamics, we recently showed via formal non-equilibrium, Berry-phase AIMD of liquid water with the same functional that liquid water's intramolecular stretch band was redshifted by some 30 and 60 cm^{-1} by 0.05 and 0.1 V/Å external static electric fields [68]. Moreover, Hermansson and Tepper gauged external electric field effects on a suite of isolated polar molecules, from weak- to strong-field conditions at the fourth-order perturbation

theory (MP4) level [69]; the level of vibrational frequency redshift increased tangibly as a function of applied field intensity.

4. Conclusions

In closing, numerical solution of the one-dimensional Schrödinger equation applied to the H_2 intramolecular stretch coordinate in extended sII hydrogen clathrate hydrate resulted in an observed redshift of ~350 cm^{-1}; this is a dramatic nuclear quantum effect, with slightly improved agreement with experimental Raman measurements relative to classical dynamics. A more subtle redshift effect appears to lie in the spatial heterogeneity of the electrostatic environment from local variation in intrinsic electric fields, which is responsible for some degree of peak splitting. It is important to remark that splitting of the fundamental H–H stretch itself was not observed in quantum calculations for a single H_2 in either a small or large hydrate cage [51,53], whilst for two H_2 molecules in a large cage, a small site-splitting of 0.5 cm^{-1} was found [53]. This discrepancy vis-à-vis more rigorous 6- and 8-D calculations [51–53] may perhaps be rationalized by rigid versus flexible cages, the use of empty hydrate cages surrounding the occupied one under Schrödinger consideration, or, indeed, possible artifacts of the originating BOMD simulations, with imperfections in the DFT functionals.

In terms of outlook for achieving greater levels of quantitative agreement relative to Raman data, ref. 45 discussed measures to potentially increase further the fidelity of H_2–water potential tailored for hydrates. In addition, it is possible that the rigorous quantum methodology for computing the H–H intramolecular stretch frequencies for double H_2 occupancy of a large cage [52,53] can be extended to three and four caged H_2 moieties. However, including cage flexibility in these calculations presents a much greater challenge.

Author Contributions: Conceptualisation, C.J.B. and N.J.E.; methodology, C.J.B., Z.F.; software, C.J.B., Z.F.; validation, C.J.B., Z.F. and N.J.E.; formal analysis, C.J.B.; investigation, C.J.B. and Z.F.; resources, N.J.E.; data curation, C.J.B.; writing—original draft preparation, C.J.B. and N.J.E.; writing—review and editing, N.J.E. and Z.B.; visualisation, C.J.B. and Z.F.; supervision, N.J.E.; project administration, N.J.E.; funding acquisition, N.J.E. and Z.B. All authors have read and agreed to the published version of the manuscript.

Funding: This research was funded by Science Foundation Ireland (N.J.E., Grant No. SFI/15/ERC/I3142), with partial support from the National Science Foundation (Z.B., Grant No. CHE-1566085).

Conflicts of Interest: The authors declare no conflict of interest.

References

1. Makogon, Y.F. *Hydrates of Hydrocarbons*; Penn Well Books: Tulsa, OK, USA, 1997.
2. Burnham, C.J.; English, N.J. Free-energy calculations of the intercage hopping barriers of hydrogen molecules in clathrate hydrates. *J. Phys. Chem. C* **2016**, *120*, 16561. [CrossRef]
3. Burnham, C.J.; Futera, Z.; English, N.J. Quantum and classical inter-cage hopping of hydrogen molecules in clathrate hydrate: Temperature and cage-occupation effects. *Phys. Chem. Chem. Phys.* **2017**, *19*, 717. [CrossRef] [PubMed]
4. Burnham, C.J.; Futera, Z.; English, N.J. Study of hydrogen-molecule guests in type II clathrate hydrates using a force-matched potential model parameterised from ab-initio molecular dynamics. *J. Chem. Phys.* under review. [CrossRef] [PubMed]
5. Trinh, T.T.; Waage, M.H.; van Erp, T.S.; Kjelstrup, S. Low barriers for hydrogen diffusion in sII clathrate. *Phys. Chem. Chem. Phys.* **2015**, *7*, 13808. [CrossRef]
6. Cendagorta, J.R.; Powers, A.; Hele, T.J.H.; Marsalek, O.; Bačić, Z.; Tuckerman, M.E. Competing quantum effects in the free energy profiles and diffusion rates of hydrogen and deuterium molecules through clathrate hydrates. *Phys. Chem. Chem. Phys.* **2016**, *18*, 32169. [CrossRef]
7. Cao, H.; English, N.J.; MacElroy, J.M.D. Diffusive hydrogen inter-cage migration in hydrogenand hydrogen-tetrahydrofuran clathrate hydrates. *J. Chem. Phys.* **2013**, *138*, 094507. [CrossRef]
8. Alavi, S.; Ripmeester, J.A. Hydrogen-Gas Migration through Clathrate Hydrate Cages. *Angew. Chem.* **2007**, *46*, 6102. [CrossRef]

9. Frankcombe, T.J.; Kroes, G.-J. Molecular Dynamics Simulations of Type-sII Hydrogen Clathrate Hydrate Close toEquilibrium Conditions. *J. Phys. Chem. C* **2007**, *111*, 13044. [CrossRef]
10. Peters, B.; Zimmerman, N.E.R.; Beckham, G.T.; Tester, J.W.; Trout, B.L. Path Sampling Calculation of Methane Diffusivity in Natural Gas Hydrates from a Water-Vacancy Assisted Mechanism. *J. Am. Chem. Soc.* **2008**, *130*, 17342. [CrossRef]
11. Gorman, P.D.; English, N.J.; MacElroy, J.M.D. Dynamical cage behaviour and hydrogen migration in hydrogen and hydrogen-tetrahydrofuran clathrate hydrates. *J. Chem. Phys.* **2012**, *136*, 044506. [CrossRef]
12. English, N.J.; MacElroy, J.M.D. Perspectives on Molecular Simulation of Clathrate Hydrates: Progress, Prospects and Challenges. *Chem. Eng. Sci.* **2015**, *121*, 133. [CrossRef]
13. Mao, W.L.; Mao, H.K.; Goncharov, A.F.; Struzhkin, V.V.; Guo, Q.; Hu, J.; Shu, J.; Hemley, R.J.; Somayazulu, M.; Zhao, Y. Hydrogen Clusters in Clathrate Hydrate. *Science* **2002**, *297*, 2247–2249. [CrossRef] [PubMed]
14. Alavi, S.; Ripmeester, J.A.; Klug, D.D. Molecular-Dynamics Study of Structure II Hydrogen Clathrate. *J. Chem. Phys.* **2005**, *123*, 024507. [CrossRef] [PubMed]
15. Mao, W.L.; Mao, H.-K. Hydrogen Storage in Molecular Compounds. *Proc. Nat. Acad. Sci. USA* **2004**, *101*, 708–710. [CrossRef]
16. Patchkovskii, S.; Tse, J.S. Thermodynamic Stability of Hydrogen Clathrate. *Proc. Nat. Acad. Sci. USA* **2003**, *100*, 14645–14650. [CrossRef]
17. Lee, J.W.; Yedlapalli, P.; Lee, S. Prediction of Hydrogen Hydrate Equilibrium by Integrating Ab Initio Calculations with Statistical Thermodynamics. *J. Phys. Chem. B* **2006**, *110*, 2332–2337. [CrossRef]
18. Sluiter, M.H.; Adachi, H.F.; Belosludov, R.V.; Belosludov, V.R.; Kawazoe, Y. Ab Initio Study of Hydrogen Storage in Hydrogen Hydrate Clathrate. *Mater. Trans.* **2004**, *45*, 1452–1454. [CrossRef]
19. Chattaraj, P.K.; Bandaru, S.; Mondal, S. Hydrogen Storage in Clathrate Hydrates. *J. Phys. Chem. A* **2011**, *115*, 187–193. [CrossRef]
20. Willow, S.Y.; Xantheas, S.S. Enhancement of Hydrogen Storage Capacity in Hydrate Lattices. *Chem. Phys. Lett.* **2012**, *525*, 13–18. [CrossRef]
21. Mao, W.L.; Koh, C.A.; Sloan, E.D. Clathrate Hydrates under Pressure. *Phys. Today* **2007**, *60*, 42–47. [CrossRef]
22. Xu, M.; Elmatad, Y.; Sebastianelli, F.; Moskowitz, J.W.; Bacic, Z. Hydrogen molecule in the small dodecahedral cage of a clathrate hydrate: Quantum five-dimensional calculations of the coupled translation-rotation eigenstates. *J. Phys. Chem. B* **2006**, *110*, 24806. [CrossRef] [PubMed]
23. Xu, M.; Sebastianelli, F.; Bacic, Z. Quantum dynamics of H_2, D_2, and HD in the small dodecahedral cage of clathrate hydrate: Evaluating H_2-water nanocage interaction potentials by comparison of theory with inelastic neutron scattering experiments. *J. Chem. Phys.* **2008**, *128*, 244715. [CrossRef] [PubMed]
24. Xu, M.; Sebastianelli, F.; Bacic, Z. Coupled translation-rotation eigenstates of H_2, HD, and D_2 in the large cage of structure II clathrate hydrate: Comparison with the small cage and rotational Raman spectroscopy. *J. Phys. Chem. A* **2009**, *113*, 7601. [CrossRef] [PubMed]
25. Powers, A.; Marsalek, O.; Xu, M.; Ulivi, L.; Colognesi, D.; Tuckerman, M.E.; Bacic, Z. Impact of the condensed-phase environment on the translation-rotation eigenstates and spectra of a hydrogen molecule in clathrate hydrates. *J. Phys. Chem. Lett.* **2016**, *7*, 308. [CrossRef]
26. Xu, M.; Felker, P.M.; Bacic, Z. Light molecules inside the nanocavities of fullerenes and clathrate hydrates: Inelastic neutron scattering spectra and the unexpected selection rule from rigorous quantum simulations. *Int. Rev. Phys. Chem.* **2020**, *39*, 425. [CrossRef]
27. Xu, M.; Ulivi, L.; Celli, M.; Colognesi, D.; Bačić, Z. Quantum Calculation of Inelastic Neutron Scattering Spectra of a Hydrogen Molecule Inside a Nanoscale Cavity Based on Rigorous Treatment of the Coupled Translation-Rotation Dynamics. *Phys. Rev. B* **2011**, *83*, 241403. [CrossRef]
28. Xu, M.; Ulivi, L.; Celli, M.; Colognesi, D.; Bačić, Z. Rigorous Quantum Treatment of Inelastic Neutron Scattering Spectra of a Heteronuclear Diatomic Molecule in a Nanocavity: HD in the Small Cage of Structure II Clathrate Hydrate. *Chem. Phys. Lett.* **2013**, *563*, 1–8. [CrossRef]
29. Colognesi, D.; Celli, M.; Ulivi, L.; Xu, M.; Bačić, Z. Neutron Scattering Measurements and Computation of the Quantum Dynamics of Hydrogen Molecules Trapped in the Small and Large Cages of Clathrate Hydrates. *J. Phys. Chem. A* **2013**, *117*, 7314–7326. [CrossRef]
30. Celli, M.; Powers, A.; Colognesi, D.; Xu, M.; Bačić, Z.; Ulivi, L. Experimental Inelastic Neutron Scattering Spectrum of Hydrogen Hexagonal Clathrate-Hydrate Compared with Rigorous Quantum Simulations. *J. Chem. Phys.* **2013**, *139*, 164507. [CrossRef]

31. Colognesi, D.; Powers, A.; Celli, M.; Xu, M.; Bačić, Z.; Ulivi, L. The HD Molecule in Small and Medium Cages of Clathrate Hydrates: Quantum Dynamics Studied by Neutron Scattering Measurements and Computation. *J. Chem. Phys.* **2014**, *141*, 134501. [CrossRef]
32. Ulivi, L.; Celli, M.; Giannasi, A.; Ramirez-Cuesta, A.J.; Bull, D.J.; Zoppi, M. Quantum Rattling of Molecular Hydrogen in Clathrate Hydrate Nanocavities. *Phys. Rev. B* **2007**, *76*, 161401. [CrossRef]
33. Giannasi, A.; Celli, M.; Zoppi, M.; Moraldi, M.; Ulivi, L. Experimental and Theoretical Analysis of Rotational Raman Spectrum of Hydrogen Molecules in Clathrate Hydrates. *J. Chem. Phys.* **2011**, *135*, 054506. [CrossRef] [PubMed]
34. Giannasi, A.; Celli, M.; Ulivi, L.; Zoppi, M. Low Temperature Raman Spectra of Hydrogen in Simple and Binary Clathrate Hydrates. *J. Chem. Phys.* **2008**, *129*, 084705. [CrossRef] [PubMed]
35. Sebastianelli, F.; Xu, M.; Bačić, Z. Quantum Dynamics of Small H2 and D2 Clusters in the Large Cage of Structure II Clathrate Hydrate: Energetics, Occupancy, and Vibrationally Averaged Cluster Structures. *J. Chem. Phys.* **2008**, *129*, 244706. [CrossRef] [PubMed]
36. Witt, A.; Sebastianelli, F.; Tuckerman, M.E.; Bačić, Z. Path Integral Molecular Dynamics Study of Small H2 Clusters in the Large Cage of Structure II Clathrate Hydrate: Temperature Dependence of Quantum Spatial Distributions. *Z. J. Phys. Chem. C* **2010**, *114*, 20775–20782. [CrossRef]
37. Felker, P.M. Fully Quantal Calculation of H2 Translation-Rotation States in (p-H2)2@51264 Clathrate Hydrate Inclusion Compounds. *J. Chem. Phys.* **2014**, *141*, 184305. [CrossRef]
38. Valdes, A.; Kroes, G.J. Theoretical investigation of two H_2 molecules inside the cages of the structure H clathrate hydrate. *J. Phys. Chem. C* **2012**, *116*, 21664. [CrossRef]
39. Felker, P.M. Fully Quantal Calculation of H2 Translation-Rotation States in (H2)4@51264 Clathrate SII Inclusion Compounds. *J. Chem. Phys.* **2013**, *138*, 174306. [CrossRef]
40. Strobel, T.A.; Sloan, E.D.; Koh, C.A. Raman Spectroscopic Studies of Hydrogen Clathrate Hydrates. *J. Chem. Phys.* **2009**, *130*, 014506. [CrossRef]
41. Wang, J.; Lu, H.; Ripmeester, J.A. Raman Spectroscopy and Cage Occupancy of Hydrogen Clathrate from First Principles Calculations. *J. Am. Chem. Soc.* **2009**, *131*, 14132–14133. [CrossRef]
42. Ramya, K.R.; Venkatnathan, A. Vibrational Raman Spectra of Hydrogen Clathrate Hydrates from Density Functional Theory. *J. Chem. Phys.* **2013**, *138*, 124305. [CrossRef] [PubMed]
43. Plattner, N.; Meuwly, M. The effect of classical and quantum dynamics on vibrational frequency shifts of H_2 in clathrate hydrates. *J. Chem. Phys.* **2014**, *140*, 02431. [CrossRef] [PubMed]
44. Zaghloul, M.A.S.; Celli, M.; Salem, N.M.; Elsheikh, S.M.; Ulivi, L. High Pressure Synthesis and In Situ Raman Spectroscopy of H2 and HD Clathrate Hydrates. *J. Chem. Phys.* **2012**, *137*, 164320. [CrossRef] [PubMed]
45. Futera, Z.; Celli, M.; del Rosso, L.; Burnham, C.J.; Ulivi, L.; English, N.J. Vibrational Modes of Hydrogen Hydrates: A First-Principles Molecular-Dynamics and Raman-Spectra Study. *J. Phys. Chem. C* **2017**, *121*, 3690–3696. [CrossRef]
46. Habershon, S.; Manolopoulos, D.E.; Markland, T.E.; Miller, T.F., 3rd. Ring-polymer Molecular Dynamics: Quantum Effects in Chemical Dynamics from Classical Trajectories in an Extended Phase Space. *Annu. Rev. Phys. Chem.* **2013**, *64*, 387–413. [CrossRef]
47. Cao, J.; Voth, G.A. The Formulation of Quantum Statistical Mechanics Based on the Feynman Path Centroid Density. II. Dynamical Properties. *J. Chem. Phys.* **1994**, *100*, 5106–5117. [CrossRef]
48. Craig, I.R.; Manolopoulos, D.E. Quantum Statistics and Classical Mechanics: Real Time Correlation Functions from Ring Polymer Molecular Dynamics. *J. Chem. Phys.* **2004**, *121*, 3368–3373. [CrossRef]
49. Hele, J.H.; Willatt, M.J.; Muolo, A.; Althorpe, S.C. Boltzmann-conserving classical dynamics in quantum time-correlation functions: Matsubara dynamics. *J. Chem. Phys.* **2015**, *142*, 134103. [CrossRef]
50. Hele, T.J.H.; Willatt, M.J.; Muolo, A.; Althorpe, S.C. Communication: Relation of centroid molecular dynamics and ring-polymer molecular dynamics to exact quantum dynamics. *J. Chem. Phys.* **2015**, *142*, 191101. [CrossRef]
51. Lauvergnat, D.; Felker, P.M.; Scribano, Y.; Benoit, D.M.; Bacic, Z. H2, HD and D2 in the small cage of structure II clathrate hydrate: Vibrational frequency shifts from fully coupled quantum six-dimensional calculations of the vibration-translation-rotation eigenstates. *J. Chem. Phys.* **2019**, *150*, 154303. [CrossRef]

52. Felker, P.M.; Bacic, Z. Weakly bound molecular dimers: Intramolecular vibrational fundamentals, overtones, and tunneling splittings from full-dimensional quantum calculations using compact contracted bases of intramolecular and low-energy rigid-monomer intermolecular eigenstates. *J. Chem. Phys.* **2019**, *151*, 024305. [CrossRef] [PubMed]
53. Felker, P.M.; Lauvergnat, D.; Scribano, Y.; Benoit, D.M.; Bacic, Z. Intramolecular stretching vibrational states and frequency shifts of (H2)2 confined inside the large cage of clathrate hydrate from an eight-dimensional quantum treatment using small basis sets. *J. Chem. Phys.* **2019**, *151*, 124311. [CrossRef] [PubMed]
54. Waldron, C.J.; English, N.J. Global-Density Fluctuations in Methane Clathrate Hydrates in Externally-Applied Electromagnetic Fields. *J. Chem. Phys.* **2017**, *147*, 024506. [CrossRef] [PubMed]
55. Waldron, C.J.; English, N.J. System-density fluctuations and electro-dissociation of methane clathrate hydrates in externally-applied static electric fields. *J. Chem. Thermo.* **2017**. [CrossRef]
56. Dion, M.; Rydberg, H.; Schröder, E.; Langreth, D.C.; Lundqvist, B.I. A density functional for sparse matter. *Phys. Rev. Lett.* **2004**, *92*, 246401. [CrossRef] [PubMed]
57. Román-Pérez, G.; Soler, J.M. Efficient implementation of a van der Waals density functional: Application to double-wall carbon nanotubes. *Phys. Rev. Lett.* **2009**, *103*, 096102. [CrossRef]
58. Wang, J.; Román-Pérez, G.; Soler, J.M.; Artacho, E.; Fernández-Serra, M.-V. Density, structure, and dynamics of water: The effect of van der Waals interactions. *J. Chem. Phys.* **2011**, *134*, 024516. [CrossRef]
59. Zhang, C.; Wu, J.; Galli, G.; Gygi, F.J. Structural and vibrational properties of liquid water from van der Waals density functionals. *Chem. Theory Comput.* **2011**, *7*, 3054. [CrossRef]
60. Corsetti, F.; Artacho, E.; Soler, J.M.; Alexandre, S.S.; Fernández-Serra, M.-V. Room temperature compressibility and diffusivity of liquid water from first principles. *J. Chem. Phys.* **2013**, *139*, 194502. [CrossRef]
61. Bankura, A.; Karmakar, A.; Carnevale, V.; Chandra, A.; Klein, M.L. Structure, dynamics, and spectral diffusion of water from first-principles molecular dynamics. *J. Phys. Chem. C* **2014**, *118*, 29401. [CrossRef]
62. English, N.J. Structural Properties of Liquid Water and Ice Ih from Ab-Initio Molecular Dynamics with a Non-Local Correlation Functional. *Energies* **2015**, *8*, 9383. [CrossRef]
63. Gillan, M.J.; Alfè, D.; Michaelides, A. Perspective: How good is DFT for water? *J. Chem. Phys.* **2016**, *144*, 130901. [CrossRef] [PubMed]
64. Nosé, S. A unified formulation of the constant temperature molecular dynamics methods. *J. Chem. Phys.* **1984**, *81*, 511. [CrossRef]
65. Garate, J.-A.; English, N.J.; MacElroy, J.M.D. Human aquaporin 4 gating dynamics in dc and ac electric fields: A molecular dynamics study. *J. Chem. Phys.* **2011**, *134*, 055110. [CrossRef]
66. Soler, J.M.; Artacho, E.; Gale, J.D.; García, A.; Junquera, J.; Ordejón, P.; Sánchez-Portal, D. The SIESTA method for ab initio order-N materials simulation. *J. Phys. Cond. Matt.* **2002**, *14*, 2745. [CrossRef]
67. Allen, M.P.; Tildesley, D.J. *Computer Simulation of Liquids*; Oxford University Press: Oxford, UK, 1987; ISBN 0470-20812-0.
68. Futera, Z.; English, N.J. Influence of external static and alternating electric fields on water from long-time non-equilibrium ab-initio molecular dynamics. *J. Chem. Phys.* **2017**, *147*, 031102. [CrossRef]
69. Hermansson, K.; Tepper, H. Electric-field effects on vibrating polar molecules: From weak to strong fields. *Mol. Phys.* **1996**, *89*, 1291–1299.